magnetochemistry

MDPI

Article

Hexakis (propargyl-*1H*-tetrazole) Iron(II) X_2 [X = BF_4, ClO_4]—Spin Switchable Complexes with Functionalization Potential and the Myth of the Explosive SCO Compound

Marco Seifried [1], Christian Knoll [1], Gerald Giester [2], Michael Reissner [3], Danny Müller [1,*] and Peter Weinberger [1,*]

1 Institute of Applied Synthetic Chemistry, Vienna University of Technology, Getreidemarkt 9/163-AC, A-1060 Vienna, Austria; marco.seifried@tuwien.ac.at (M.S.); christian.knoll@tuwien.ac.at (C.K.)
2 Faculty of Geosciences, Geography and Astronomy, University of Vienna, Althanstraße 14 (UZA 2), A-1090 Vienna, Austria; gerald.giester@univie.ac.at
3 Institute of Solid State Physics, Vienna University of Technology, Wiedner Hauptstraße 8-10/138, A-1040 Vienna, Austria; reissner@ifp.tuwien.ac.at
* Correspondence: danny.mueller@tuwien.ac.at (D.M.); weinberg@mail.zserv.tuwien.ac.at (P.W.); Tel.: +43-1-58801-163740 (D.M.); +43-1-58801-163617 (P.W.); Fax: +43-1-58801-16299 (D.M. & P.W.)

Academic Editors: Guillem Aromí and José Antonio Real
Received: 14 January 2016; Accepted: 14 February 2016; Published: 26 February 2016

Abstract: Spin crossover complexes with ligands suitable for further functionalization could allow for an easy access to multifunctional switchable materials. Within this context, we recently characterized the Fe(II) SCO complexes of propargyl-*1H*-tetrazole. Although the design of the ligand seems similar to the one of the well-known propyl-*1H*-tetrazole, the spin transition behavior is notably different. Both compounds reported herein feature a gradual spin transition with a $T_{1/2}$ shifted to lower temperatures, compared to the more flexible propyl-ligand. Due to the potential instable structure of these compounds, especially of the perchlorate complex, we also investigated our compounds with regard to their sensitivity against thermal and mechanical stress. These experiments led to the conclusion that the proper handling includes no enhanced risk of explosive decomposition.

Keywords: spin crossover; iron; tetrazole; post-functionalization; DFT

1. Introduction

Design and investigation of magnetic materials with sensitivity to external influences, affecting their magnetic moment and/or properties attract notable interest due to their potential applications. Within this context, especially the spin transition of d^4-d^7 transition metals on external perturbations such as temperature, light, pressure, nuclear decay, magnetic field, *etc.* [1–6] is considered suitable for future technological use of these materials in, e.g. switching, sensing, or memory devices [7–12].

Referring to potential technological applicability of the spin crossover (SCO) effect, within the 84 years after the discovery of the spin crossover effect [13,14], two milestones should be highlighted. The first refers to the discovery of the LIESST (light induced excited spin state trapping) effect [15–17] by Decurtins and coworkers. Although the LIESST effect was restricted for a long time to low temperatures, 10 years ago Bousseksou and coworkers reported about a reversible one-shot spin state conversion at room-temperature [18]. A second milestone was the presentation of the first SCO-based display device by Kahn and Martinez [7], a monochrome display using the thermochromic effect

of SCO compounds. In combination, these two examples are illustrative for the always mentioned potential applicability of SCO materials.

To keep up with today's technological demands, combinations of the SCO effect with additional properties would be appealing. Therefore, a recent trend is the introduction of multifunctionality to SCO in the form of, e.g. ligand isomerism [6], luminescence [19,20], nonlinear optics [21], or host-guest chemistry [22–24], thus allowing for a broader scope of possible applications.

One concept for the introduction of multifunctionality that our group recently started to investigate is the post-functionalization of suitable SCO complexes. This approach is based on the strategy of avoiding time-consuming ligand design by having one suitable "platform", allowing for quick and easy further functionalization according to the respective demands. In this context, the use of a ligand with a carbon-carbon triple bond was considered a proper structural motif.

Herein, we report the synthesis and characterization of two Fe(II) SCO complexes based on the propargyl-*1H*-tetrazole ligand (prgTz).

2. Results and Discussion

Comparing the series of alkyl-substituted N1-tetrazole Fe(II) SCO-complexes [25], the very first tetrazole-Fe(II) SCO complex [Fe(1-propyl-*1H*-tetrazole)$_6$]$^{2+}$ (3tz) [26,27] reported by Gütlich and coworkers features the most abrupt and complete spin transition, even with a small hysteresis ($T_{1/2}^{\downarrow}$ = 128 K, $T_{1/2}^{\uparrow}$ = 135 K). Therefore, the choice of the prgTz-ligand was also driven by the idea to obtain a comparably sharp and abrupt SCO behavior as for the propyl compound.

As is known, different anions have a notable impact on the SCO behavior because of their different size and thus density of the molecular packing. [28,29] Subsequently, [Fe(prgTz)$_6$](X)$_2$, X = BF_4 (**1**) or ClO_4 (**2**), are compared.

2.1. Magnetic Properties

Magnetic susceptibility measurements were performed on powder samples of **1** and **2** in a range of 10–300 K. In Figure 1, the $\chi_{mol}T$ *vs.* T plot, contrasting the magnetic behavior of the prgTz-complexes to the one of the [Fe(1-propyl-*1H*-tetrazole)$_6$](BF_4)$_2$, is represented.

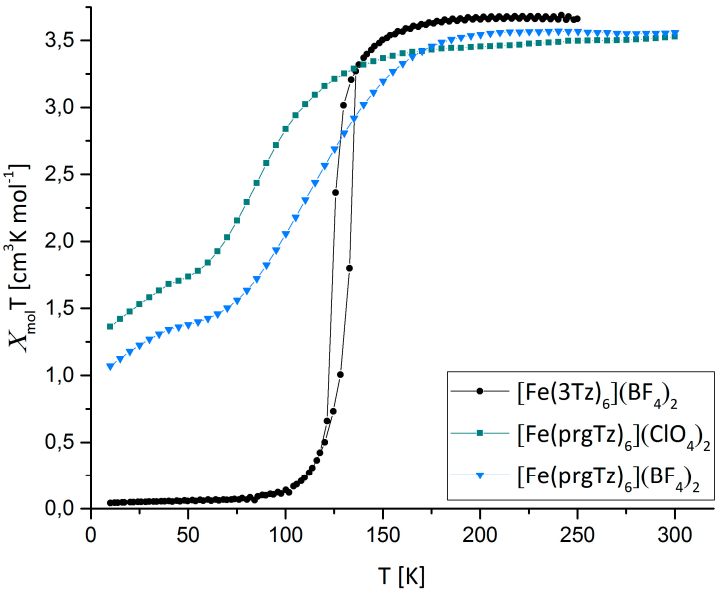

Figure 1. Temperature dependence of $\chi_{mol}T$ for **1** (blue), **2** (green) and [Fe(3tz)$_6$](BF_4)$_2$ (black) [26,27].

Instead of an up-shift of $T_{1/2}$ due to the enhanced rigidity of the prgTz ligand, cooperativity is lost, leading to a gradual, incomplete spin transition located below the one of the 3tz compound.

At room-temperature, both **1** and **2** display a $\chi_{mol}T$ value of 3.5, which is in perfect agreement with the expectations for an Fe(II) in the high-spin (HS)-state. For the BF_4-complex **1**, a decrease of the magnetic moment, beginning at 185 K to a final value of 1.04 at 10 K is observed, whereas for the ClO_4-complex **2**, the spin transition initiates at 143 K, leading to a final $\chi_{mol}T$ value of 1.31 at 10 K.

In terms of absolute figures, **1** has a $T_{1/2}$ of 120 K with 21% of the Fe-atoms remaining in the HS state, whereas **2** displays a notably lower $T_{1/2}$ of 97 K with 27% residual HS-fraction. Especially, the incomplete spin-transition is notable, as the only difference to the 3tz, with its abrupt and hysteretic SCO behavior, is the reduced conformational flexibility of the ligand.

The second decrease of the magnetization for both compounds located below 50 K may be attributed to the zero field splitting.

2.2. Molecular Structure

All attempts to obtain single crystals, suitable for structural determination, failed. Therefore, structural information was achieved by determination of the molecular structure of the homologous Ni-complex. The violet hexagonal platelets obtained via diffusion crystallization also revealed to be highly twinned and disordered. The irregular shape of the platelets is exemplified in the scanning electron microscope (SEM)-picture of **1** (see Figure 2). A comparison of the mid-infrared (MIR) spectra of **1** and its Ni-homolog, confirming their analogy, is found in the supporting information (SI) (see Figure S1).

Figure 2. SEM picture of $[Fe(prgTz)_6](BF_4)_2$ at 298 K, magnification 1500 times.

Therefore, only poor structural data could be obtained. In Figure 3, the Oak Ridge Thermal Ellipsoid Plot (ORTEP) of $[Ni(prgTz)_6](BF_4)_2$ is represented. Hydrogen atoms are omitted for clarity.

The **1** homologous $[Ni(prgTz)_6](BF_4)_2$ complex crystallizes in the trigonal space group $R\bar{3}$ with two different Ni-positions with both Ni-N_6 octahedra showing almost regular octahedral coordination.

The detailed crystallographic data for $[Ni(prgTz)_6](BF_4)_2$ are given in Table 1.

For Ni(1), the three ligands are not crystallographically equivalent due to their different alignments of the propargyl-chain. For Ni(2), all six ligands show the same spatial alignment, thus are crystallographically equivalent. The fluorine atoms of the BF_4-anions are disordered, thus leading to two different anion orientations each. Both BF_4 groups were refined with split models fixing the sum of occupancy to be one with distribution ratios of 0.78:0.22 and 0.85:0.15 for $B(1)F_4$ and $B(2)F_4$, respectively. Hydrogen atoms were put on idealized positions (riding model).

In Table 2, selected bond lengths and angles for $[Ni(prgTz)_6](BF_4)_2$ are given.

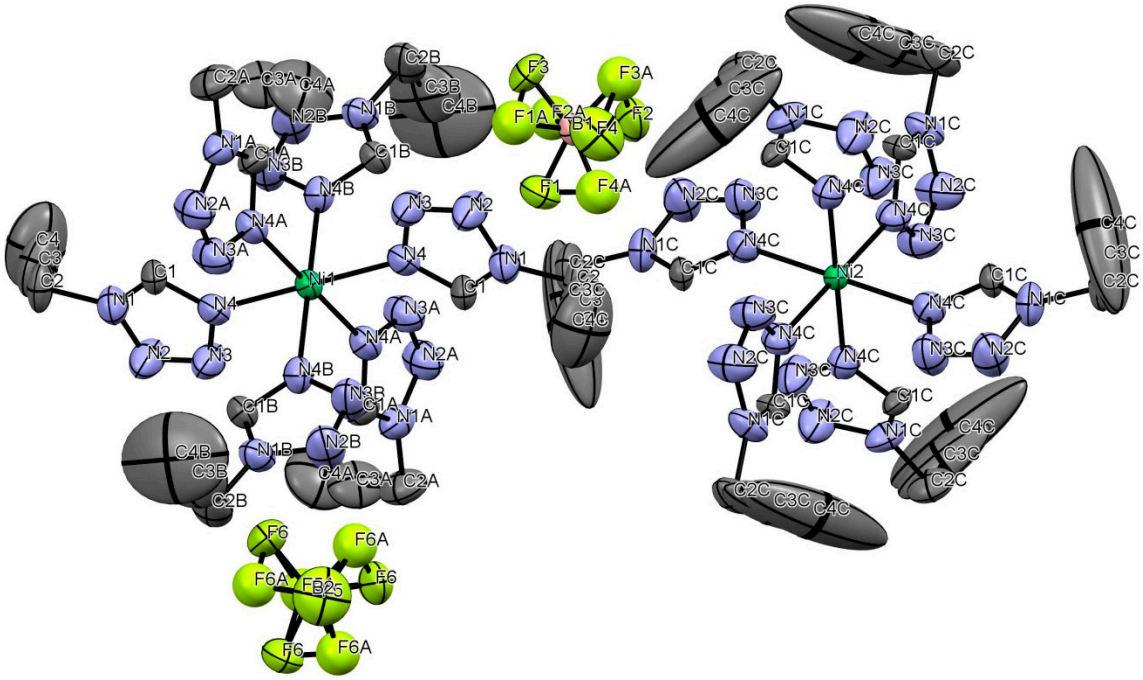

Figure 3. ORTEP-drawing of $[Ni(prgTz)_6](BF_4)_2$ at 200 K with atomic labeling. Displacement ellipsoids are given at 50% probability level. BF_4 groups are disordered.

Table 1. Selected crystallographic data for $[Ni(prgTz)_6](BF_4)_2$ at 200 K.

Empirical Formula	**$C_{24}H_{21}B_2F_8N_{24}Ni$**	**FW**	**877.89**
Z=	12	Space group	$R\bar{3}$
λ=	0.71073 Å	*T*, K	200
a, Å	20.221(2)	-	-
c, Å	35.398(4)	-	-
V, Å^3	12534.7	$_{calc,}$ g·cm^{-3}	1.396
Final R1	0.102	Final wR2	0.37

Table 2. Selected bond lengths and angles for $[Ni(prgTz)_6](BF_4)_2$ at 200 K. Estimated standard deviations of bond lengths are ~0.006 Å.

Atom Number	**Bond length [Å]**	**Atom Number**	**Angles [deg]**
Ni(1)–N4	2.110	N4–Ni(1)–N4	180.00
Ni(1)–N4A	2.089	N4C–Ni(2)–N4C	180.00
Ni(1)–N4B	2.095	N4–Ni(1)–N4A	89.78
Ni(2)–N4C	2.083	N4–Ni(1)–N4B	90.59
N2–N3	1.302	N4C–Ni(1)–N4C	90.69
N2A–N3A	1.287	-	-
N2B–N3B	1.271	-	-
N2C–N3C	1.296	-	-

2.3. Variable Temperature Spectroscopy

Especially, for Fe(II) tetrazole SCO systems variable temperature spectroscopy can be used as valuable complementary analysis supporting the data obtained from magnetic and structural characterization.

2.3.1. MIR-Spectroscopy

The changes in the bond strength between the Fe atom and the coordinating N4 upon a spin transition are observed according to the shift of the peak position in the MIR-spectra. The variable temperature MIR spectra of **(1)** are shown in Figure 4, for **(2)** in Figure S2.

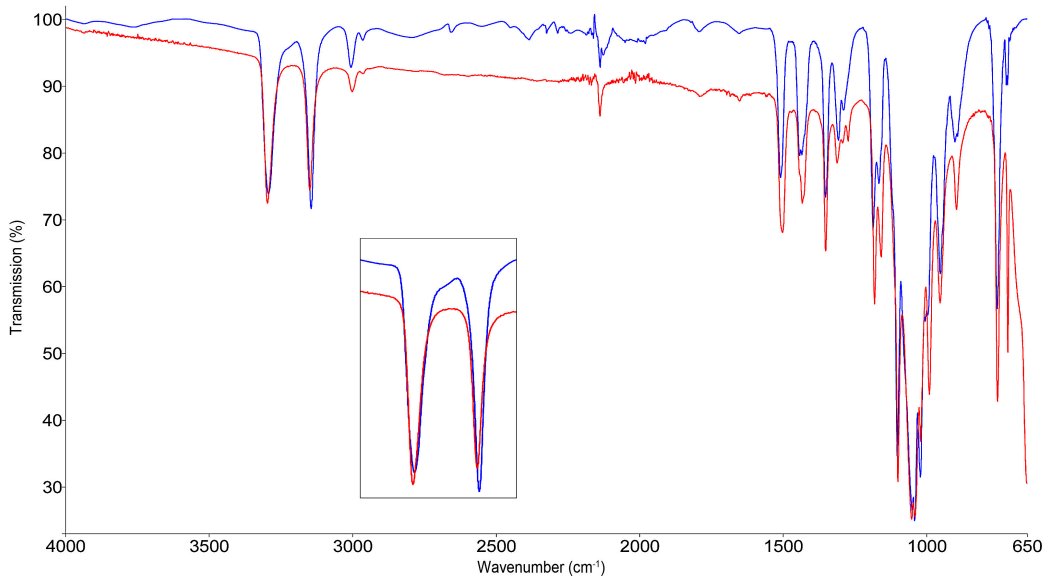

Figure 4. Variable temperature mid-infrared spectra of **1**, high-spin state at 300 K (red) and partial low-spin state at 100 K (blue).

Due to the vicinity of the tetrazolic $_{CH}$ to the coordinating N4 upon cooling to 100 K, a shift from 3149 cm^{-1} to 3146 cm^{-1} is observed. The shift towards lower wavenumbers can be explained with an electronic effect, exhibited on the tetrazole ring by the strengthening of the Fe-N bond length in the LS-state. The MIR spectra of **1** for both spin-states are represented above.

The same effect is observed for the vibrational mode of the alkyne-proton, also displaying a shift of 3 cm^{-1} to lower wavenumbers in the low-spin (LS). Due to the conjugation of the ligand, the electronic impact of the SCO is translocated over six atoms.

The in-plane vibrations of the tetrazolic CN- (1500 cm^{-1}) and N-N-N-motif (1181 cm^{-1}) show the same, but weaker shift.

2.3.2. FIR-Spectroscopy

The motion of the iron atom towards the N-N-N-planes of the nitrogen coordination octahedron can be distinguished for both spin-states in the far-infrared (FIR) [30]. For the spectrum obtained at low-temperatures, the rise of a broad band at 467 cm^{-1} is observed, corresponding to the LS Fe-motion. The band for the HS Fe vibration at 267 cm^{-1} shows only a slight decrease of intensity, attributed to the incomplete spin transition (see Figure 5). The FIR-spectra for **(2)** are given in Figure S3.

It is obvious that the direct observation of the Fe-N motion, featuring the two correlated bands in the FIR, is a more sensitive indicator for the SCO than the indirect detection by observation of the tetrazolic ν_{CH} vibration in the MIR spectrum. Especially for incomplete spin transitions, the rather small shift of the MIR bands allows for no unambiguous determination of the ratio of LS to HS fraction.

2.3.3. Visible/Near-Infrared (VIS/NIR)-Spectroscopy

The characteristic magenta color for the N_6-iron system is caused by different electronic d-d transitions of the metal center. The HS species have a characteristic broad absorption in the near infrared region with a maximum located at 887 nm. This corresponds to a $^5T_{2g} \rightarrow {}^5E_g$ transition,

invisible to the human eye. Concomitant to the decrease in temperature the intensity of the NIR band also decreases, which is correlated to the increase of the characteristic LS absorption band of the $^1A_{1g} \rightarrow {}^1T_{1g}$ transition at 556 nm.

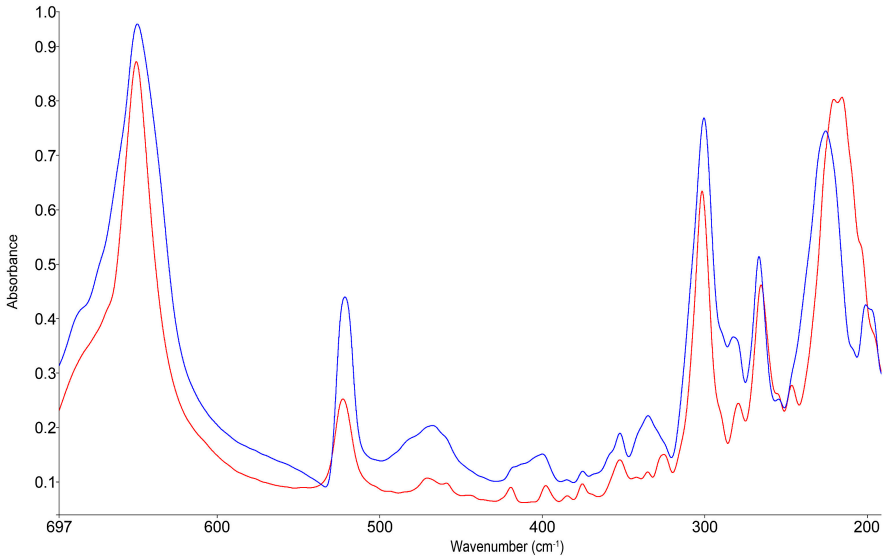

Figure 5. Variable temperature far-infrared spectra of **1**, HS state at 300 K (red) and partial LS state at 100 K (blue).

In Figure 6, the blue spectrum represents a partial LS state at 130 K, as seen by the remaining intensity of the HS band. This perfectly correlates to the data obtained from the magnetic measurements, as well as from the FIR spectra.

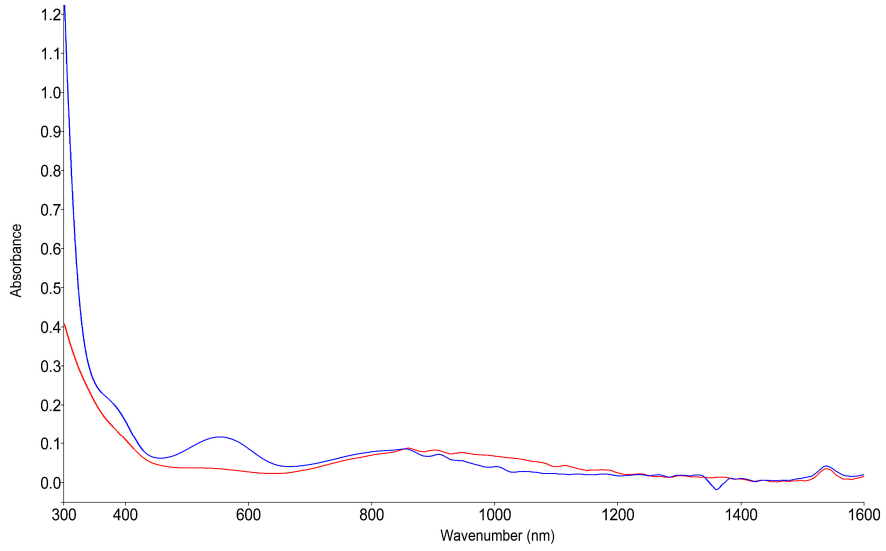

Figure 6. Variable temperature visible/near-infrared spectra of **1**, HS state at 300 K (red) and partial LS state at 130 K (blue).

Due to its similarity to the already presented data, the spectroscopic data for **2** are shown in the Supplementary Material (see Figure S4).

2.4. Post-Functionalization of the prgTz Complexes

The quest for applicability of SCO compounds sheds light on possible multifunctional materials. The intention for the current ligand design was based on the necessity of introducing a reactive group to the ligand that would not interfere with coordination, while allowing for subsequent further modifications. Such a strategy would prove advantageous, as once having a suitable platform, a quick screening of various substrates bearing an additional property is enabled.

The carbon-carbon triple bond in our ligand should allow for application of standard protocols like alkyne-metathesis or a click reaction. The latter can especially be regarded as highly suitable for this purpose, as similar examples of post-functionalization of complexes are known in the literature [31–33].

With first very promising results in hand, the synthetic protocols, and especially the characterization of the resulting functionalized complexes, is currently ongoing in our group and will be subject of a future, follow-up report on this work.

2.5. Thermal and Mechanic Sensitivity

At the beginning of our work on a small tetrazole ligand with a reactive triple bond, and especially in combination with a perchlorate anion, we came up with the question about potential safety issues on handling of these compounds. Therefore, different investigations exhibiting mechanic and thermal stress on the compounds were performed.

Introducing both BF_4-(**1**) and ClO_4-(**2**) complexes to the flame of a Bunsen-burner leads to inflammation of the compound, but without any visible or audible evidence of explosive decomposition.

The thermogravimetric analysis of **1** in nitrogen atmosphere (see Figure 7a) shows a slow and incomplete decomposition of the sample with an onset of 433.7 K. The mass-loss corresponds to 38.6%.

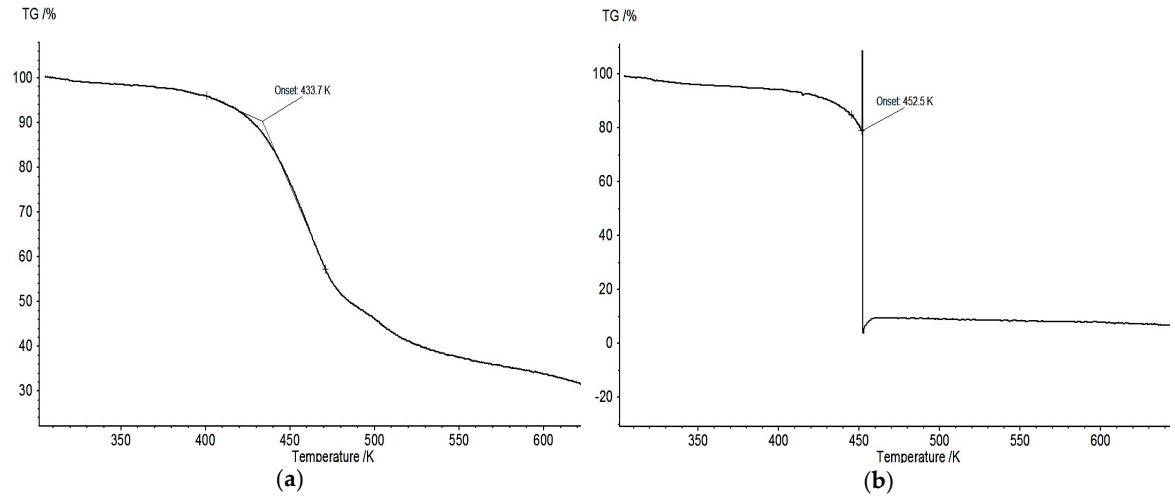

Figure 7. (**a**) Thermogravimetric analysis of BF_4-complex **1**; and (**b**) TGA curve of ClO_4-complex **2**.

In contrast, for the ClO_4-complex **2**, above 452.5 K, an immediate decomposition with a mass-loss of 80.4% is observed (see Figure 7b). The much more complete decomposition compared to **1** can be attributed to the presence of the perchlorate as oxidant. Although the decomposition is very abrupt, no acoustic noise characteristic for an explosive decomposition could be registered.

To assess the tolerance of the compound against mechanic stress, a drop hammer setup was used [34]. For neither the BF_4- nor the ClO_4-complex in repeated tests with varying amounts of substance any reaction was observed, as also evidenced by MIR-analysis of the residue. That led to the conclusion that both **1** and **2** are insensitive towards impacts with kinetic energies up to 14.7 J (*i.e.*, dropping 1 kg from the height of 150 cm).

To deduce any pressure sensitivity, **1** and **2** were treated in a hydraulic press with a maximum load of 11 tons. Similar to the drop hammer, no change was observed on MIR analysis of the residues here.

Although our investigations of the respective compounds towards shock and thermal sensitivity resulted in astonishing stability, we explicitly warn against deducing from these experiments that all tetrazole perchlorate compounds can be handled without any risk. Nevertheless, a safe handling of similar compounds is possible, but needs to be tested individually for each case, especially as all reported experiments herein were carried out at a mg scale. Therefore, the authors take no responsibility for any accident when working with the reported compounds.

Nevertheless, with regard to these results, we want to emphasize that the use of tetrazoles as ligands, and also the combination with a perchlorate anion, does not automatically state the compounds as explosives. We hope that this work can contribute to the discussion about the risks of investigating azole-SCO systems, breaking the myth of the predominantly explosive nature of tetrazole-SCO compounds.

2.6. Theoretical Modeling

The DFT calculations were performed using Gaussian 09 (Version 09 Rev. D01, Gaussian, Inc, Wallingford, CT, USA, 2013) implemented on the Vienna Scientific Cluster 3 (Version 3, Vienna Scientific Cluster, c/o Zentraler Informatikdienst, High Performance Computing, Vienna University of Technology, Vienna, Austria, 2014). The structure of the ligand was drawn using GaussView (Version 5.0.8, Gaussian, Inc, Wallingford, CT, USA, 2000–2008), followed by a molecular mechanics structure optimization implemented in the software package. For the complex, the molecular structure was imported from the single crystal X-ray analysis.

The calculations were run using density functional theory with the hybrid functional B3LYP [35–37] for structure optimization to a ground state. Literature dealing with DFT calculations of iron(II) spin crossover compounds revealed that this functionality is able to fit experimental data quite well [38–40]. One possible adjustment to get better agreement to experimental data is the change of the exact exchange contribution from 20% in B3LYP to 15%, which is known as the Becke, 3-parameter, Lee-Yang-Parr (B3LYP)* functional [41].

In order to keep computational cost within a reasonable range, the first optimization towards a local minimum was carried out using the SDD basis set. Upon convergence, the 6-311+g valence triple zeta basis set [42] with polarization and diffuse functions was used for refining the structure and calculation of vibrational modes to prove the discovery of a local minimum.

The calculated spectra are uncorrected and used as provided from the output file. No imaginary frequencies were obtained. In Table 3, important vibrational modes are compared. Their absolute values differ from experimental findings, but the difference between high spin and low spin state is in the range of experimental values. To achieve a numerical accordance between the calculated and experimental results, an empirical correction would be needed. This has been avoided so far, as the main objective of the calculation was the full-vibrational analysis, thus allowing for better assignment and explanation of the vibrations affected by the SCO.

Table 3. Comparison of calculated and experimental infrared-shifts (Δ_ν) upon spin transition.

Vibration	LS exp. (cm^{-1})	HS exp. (cm^{-1})	(Δ_ν) exp. (cm^{-1})	LS calc. (cm^{-1})	HS calc. (cm^{-1})	(Δ_ν) calc. (cm^{-1})
$\nu_{(CNTz)}$	1507	1500	−7	1441	1436	−5
$\nu_{(C\equiv C)}$	2140	2140	0	2222	2222	0
$\nu_{(CHTz)}$	3146	3149	+3	3308	3304	−4
$\nu_{(\equiv CH)}$	3294	3297	+3	3454	3454	0

The coordinates of the calculated low-spin structure for the $[Fe(prgTz)_6]^{2+}$ cation (Table S1) and of the calculated high-spin structure for the $[Fe(prgTz)_6]^{2+}$ cation (Table S2) are available in the supporting information.

3. Experimental Section

3.1. General Methodology

For the synthesis of the ligand via Franke procedure [27], all starting materials and solvents were used in commercial available quality without further purification. All complexations were performed under an inert atmosphere of argon using Schlenk techniques. The solvents were dried and degassed before use [43] and stored over molecular-sieve 3 Å under argon. Single crystals suitable for structural characterization were obtained by diffusion crystallization.

Caution: Although no risks in handling the reported materials were encountered, proper and careful treatment is highly recommended!

3.2. Sample Analysis

^1H and ^{13}C [^1H] NMR spectra were recorded on a Bruker 400 spectrometer (Bruker Corporation, 40 Manning Road, Billerica, MA, USA) with broad-band probe head. All NMR chemical shifts are reported in ppm; ^1H and ^{13}C shifts are established on the basis of the residual solvent resonance.

Mid-range IR spectra were recorded in attenuated total reflection (ATR) technique within the range of 4000–450 cm^{-1} using a Perkin-Elmer Spectrum Two Fourier-transform infrared spectrometer (PerkinElmer Inc., 940 Winter St., Waltham, MA, USA). Low-temperature mid and far IR spectra were recorded using a Perkin-Elmer 400 FIR/MIR FTIR spectrometer fitted with a Gladi-ATR-unit with liquid nitrogen as cooling agent.

Electronic spectra of the undiluted powder samples have been measured using a Perkin Elmer Lambda 900 UV-VIS-NIR spectrometer equipped with a thermostatable powder sample holder in diffuse reflection geometry (Praying Mantis accessory®, Harrick Scientific Products Inc, Pleasantville, NY, USA) between 300 nm and 1200 nm.

The magnetic moment of the Fe(II)-complexes was measured using a Physical Property Measurement System (PPMS®) by *Quantum Design* (Quantum Design, Inc., 6325 Lusk Boulevard, San Diego, CA, USA). The experimental setup consisted of a vibrating sample magnetometer attachment (VSM), bearing a brass-sample holder with a quartz glass powder container. The moment was determined in an external field of 1 T in the range of 10 K to 400 K. A final diamagnetic correction was applied.

$T_{1/2}$ refers to the temperature, where 50% of the overall-switchable molecular fraction of Fe^{2+}-ions is in the LS-state.

The powder X-ray diffraction measurements were carried out on a Panalytical X'Pert diffractometer (PANalytical B.V., Lelyweg 1, Almelo, The Netherlands) in Bragg-Brentano geometry using Cu K_α radiation (λ = 1.542 Å), an X'Celerator linear detector (PANalytical B.V., Lelyweg 1, Almelo, The Netherlands) with a Ni-filter, sample spinning and $2\theta = 5^\circ$–70°, T = 297 K.

Single crystals were attached to a glass fiber using perfluorinated oil and mounted on a Bruker KAPPA APEX II diffractometer equipped with a charge-coupled device (CCD) detector. Data were collected at 200 K (Cryostream 800, Oxford Cryosystems, Oxford Cryosystems Ltd, 3 Blenheim Office Park, Long Hanborough, Oxford OX29 8LN, United Kingdom) in a dry stream of nitrogen with Mo K_α radiation (Incoatec Microfocus Source IμS: 30 W, multilayer mirror, λ = 0.71073 Å). Redundant datasets were collected. Frame data were reduced to intensity values using SAINT-Plus [44] and an absorption correction was applied using the multi-scan method implemented by SADABS [44]. The structures were determined by direct methods and refined with SHELXS-97 and SHELXL-97, respectively [45,46].

Thermogravimetric analyses were performed on a Netzsch TG 209-C (Erich NETZSCH GmbH & Co. Holding KG, Gebrüder-NETZSCH-Straße 19, Selb, Germany) in an Al_2O_3 crucible at a heating rate of 10 K·min^{-1} in a nitrogen atmosphere.

For the drop hammer experiments, a construction similar to the one described in the literature [34] with a hammer weight of 1 kg and a maximum dropping-height of 150 cm was used.

3.3. Ligand Synthesis

Propargyl-*1H*-tetrazole

The ligand propargyl-*1H*-tetrazole (prgTz) was synthesized according to the procedure reported by our group [47].

Propargylamine (21.6 g, 392 mmol, 1 eq.), sodium azide (38.2 g, 588 mmol, 1.5 eq) and triethylorthoformate (90 g, 608 mmol, 1.55 eq) were dissolved in 100 mL glacial acetic acid and the mixture was stirred at 90 °C for 21 h. The solvent was evaporated under reduced pressure, the residue dissolved in 300 mL 2 M HCl, and this solution was extracted with ethyl acetate. After washing the organic phase with saturated $NaHCO_3$-solution and saturated NaCl-solution, the combined extracts were dried over $MgSO_4$ and the solvent was evaporated under reduced pressure. The residue was purified via bulb-to-bulb distillation (0.0025 mbar, 130–150 °C) to afford 19 g (45%) of slightly yellow oil with a density of 1.185 g/cm^3.

^{1}H NMR (400 MHz, $CDCl_3$): δ = 8.95 (s, 1H, C*H*(Tz)), 5.21 (d, *J* = 2.8 Hz, 2H, –CH_2–), 2.64 (t, *J* = 2.7 Hz, 1H, –C*H*) ppm.

^{13}C NMR (101 MHz, $CDCl_3$): δ = 142.74 (s, Tz), 76.51 (s, alkyne), 73.77 (s, alkyne), 37.85 (s, CH_2) ppm.

IR (ATR): 3280 ($_{HC\equiv C}$), 3138 ($_{(CHTz)}$), 2980 ($_{CH2}$), 2134 ($_{C\equiv C}$), 1481 ($_{(CNTz)}$), 1100 ($_{Tz}$) cm^{-1}.

3.4. Complexation Reactions

3.4.1. $[Fe(prgTz)_6](BF_4)_2$ (1)

PrgTz (300 mg, 2.78 mmol, 6 eq.) and anhydrous $Fe(BF_4)_2$ (112 mg, 0.46 mmol, 1 eq.) were dissolved in 5 mL acetonitrile and stirred at 50 °C for 18 h. The solvent was evaporated under reduced pressure and the residue washed twice with dichloromethane. After drying in vacuum, 300 mg (75%) of (**1**) were isolated as a white powder.

IR (ATR): 3297 ($_{HC\equiv C}$), 3149 ($_{(CHTz)}$), 2994 ($_{CH2}$), 2140 ($_{C\equiv C}$), 1500 ($_{(CNTz)}$), 1052 ($_{Tz}$) cm^{-1}.

3.4.2. $[Fe(prgTz)_6](ClO_4)_2$ (2)

PrgTz (300 mg, 2.78 mmol, 6 eq.) was stirred with $Fe(ClO_4)_2{\cdot}6H_2O$ (170 mg, 0.463 mmol, 1 eq.) in 5 mL acetonitrile at 50 °C for 18 h. Prior to the addition, $Fe(ClO_4)_2{\cdot}6H_2O$ was stirred for 10 min with a tip of a spatula of ascorbic acid to remove traces of Fe^{3+}. After evaporation of the solvent, the residue was washed with dichloromethane and subsequently dried in vacuum, yielding (**2**) as off-white powder (400 mg, 86%).

IR (ATR): 3293 ($_{HC\equiv C}$), 3139 ($_{(CHTz)}$), 2994 ($_{CH2}$), 2139 ($_{C\equiv C}$), 1501 ($_{(CNTz)}$), 1082 ($_{Tz}$) cm^{-1}.

4. Conclusions

Within this work, we reported on our investigations of two iron(II) SCO compounds derived from the propargyl-1H-tetrazole ligand. Both a BF_4^- and a ClO_4^-complex were characterized, featuring incomplete spin transitions with a $T_{1/2}$ of 120 K (21% residual HS-state) for **1** and a $T_{1/2}$ of 97 K (27% residual HS-state) for **2**.

First attempts of post-functionalization of the complexes using the alkyne functionality led to promising results, which are the subject of further ongoing investigations.

Repeated experiments were performed to assess the possible risks of handling unsaturated tetrazole-SCO complexes, even in combination with a ClO_4^- anion. They resulted in no evidence for any explosive decomposition, neither under thermal nor mechanical stress. Although we warn from an extrapolation of these results to any similar compounds, these results clearly contrast the wide-spread assumption of explosive Fe(II)-tetrazole SCO materials.

Supplementary Materials: The following are available online at www.mdpi.com/2312-7481/2/1/12/s1, Figure S1: Comparison of the mid-infrared spectra for $[Fe(prgTz)_6](BF_4)_2$ (red) and $[Ni(prgTz)_6](BF_4)_2$ (black), Figure S2: Mid-infrared spectrum of $[Fe(prgTz)_6](ClO_4)_2$, high-spin (red) and low-spin (blue), Figure S3: Far-infrared spectrum of $[Fe(prgTz)_6](ClO_4)_2$, high-spin (red) and low-spin (blue), Figure S4: Visible/near-infrared spectrum of $[Fe(prgTz)_6](ClO_4)_2$, high-spin (red) and low-spin (blue), Table S1: Coordinates of the calculated low-spin structure for the $[Fe(prgTz)_6]^{2+}$ cation, Table S2: Coordinates of the calculated high-spin structure for the $[Fe(prgTz)_6]^{2+}$ cation.

Acknowledgments: Thanks for financial support to the Austrian Science Fund (FWF Der Wissenschaftsfond) project P24955-N28. The computational results presented have been achieved using the Vienna Scientific Cluster. Thanks are also due to the X-ray center of Vienna University of Technology (Klaudia Hradil). This work was performed in the framework of the Cooporation in Science and Technology (COST) action CM1305 "Explicit Control Over Spin-states in Technology and Biochemistry (ECOSTBio).

Author Contributions: Marco Seifried performed the synthesis and spectroscopic characterization. Christian Knoll was responsible for theoretical modeling of the compounds. Gerald Giester performed the crystallographic characterization. Michael Reissner did the magnetic susceptibility measurements. Danny Müller was responsible for conception and writing of the article. Peter Weinberger is the head of the working group, and proofread and co-wrote the article.

Conflicts of Interest: The authors declare no conflict of interest.

References

1. Gütlich, P.; Goodwin, H.A. Spin crossover in transition metal compounds I. In *Topics in Current Chemistry*; Springer: Berlin, Heidelberg, Germany, 2004.
2. Real, J.A.; Gaspar, A.B.; Niel, V.; Munoz, M.C. Communication between iron(II) building blocks in cooperative spin transition phenomena. *Coord. Chem. Rev.* **2003**, *236*, 121–141. [CrossRef]
3. Goodwin, H.A. Spin transitions in 6-coordinate iron(II) complexes. *Coord. Chem. Rev.* **1976**, *18*, 293–325. [CrossRef]
4. Gütlich, P.; Garcia, Y.; Goodwin, H.A. Spin crossover phenomena in Fe(II) complexes. *Chem. Soc. Rev.* **2000**, *29*, 419–427. [CrossRef]
5. Gütlich, P.; Hauser, A.; Spiering, H. Thermal and optical switching of iron(II) complexes. *Angew. Chem. Int. Ed.* **1994**, *33*, 2024–2054. [CrossRef]
6. Boillot, M.L.; Pillet, S.; Tissot, A.; Riviere, E.; Claiser, N.; Lecomte, C. Ligand-driven light-induced spin change activity and bidirectional photomagnetism of styrylpyridine iron(II) complexes in polymeric media. *Inorg. Chem.* **2009**, *48*, 4729–4736. [CrossRef] [PubMed]
7. Kahn, O.; Martinez, C.J. Spin-transition polymers: From molecular materials toward memory devices. *Science* **1998**, *279*, 44–48. [CrossRef]
8. Loutete-Dangui, E.D.; Varret, F.; Codjovi, E.; Dahoo, P.R.; Tokoro, H.; Ohkoshi, S.; Eypert, C.; Letard, J.F.; Coanga, J.M.; Boukheddaden, K. Thermal spin transition in $[Fe(NH_2\text{-}trz)_3]Br_2$ investigated by spectroscopic ellipsometry. *Phys. Rev. B* **2007**, *75*. [CrossRef]
9. Bousseksou, A.; Molnar, G.; Demont, P.; Menegotto, J. Observation of a thermal hysteresis loop in the dielectric constant of spin crossover complexes: Towards molecular memory devices. *J. Mater. Chem.* **2003**, *13*, 2069–2071. [CrossRef]
10. Mounaix, P.; Freysz, E.; Degert, J.; Daro, N.; Letard, J.F.; Kuzel, P.; Vigneras, V.; Oyenhart, L. One-dimensional tunable photonic crystals with spin crossover material for the terahertz range. *Appl. Phys. Lett.* **2006**, *89*. [CrossRef]
11. Van Koningsbruggen, P.J.; Garcia, Y.; Kahn, O.; Fournes, L.; Kooijman, H.; Spek, A.L.; Haasnoot, J.G.; Moscovici, J.; Provost, K.; Michalowicz, A.; *et al*. Synthesis, crystal structure, EXAFS, and magnetic properties of catena [μ-Tris(1,2-bis(tetrazol-1-yl)propane-*N*1,*N*1′)iron(II)] Bis(perchlorate). First crystal structure of an iron(II) spin-crossover chain compound. *Inorg. Chem.* **2000**, *39*, 1891–1900. [CrossRef] [PubMed]

12. Bousseksou, A.; Molnar, G.; Salmon, L.; Nicolazzi, W. Molecular spin crossover phenomenon: Recent achievements and prospects. *Chem. Soc. Rev.* **2011**, *40*, 3313–3335. [CrossRef] [PubMed]
13. Cambi, L.; Szego, L. The magnetic susceptibility of complex compounds. *Ber. Dtsch. Chem. Ges.* **1931**, *64*, 2591–2598. [CrossRef]
14. Cambi, L.; Szego, L. The magnetic susceptibility of complex compounds (II report). *Ber. Dtsch. Chem. Ges.* **1933**, *66*, 656–661. [CrossRef]
15. Decurtins, S.; Gütlich, P.; Kohler, C.P.; Spiering, H.; Hauser, A. Light-induced excited spin state trapping in a transition-metal complex—The hexa-1-propyltetrazole-iron (II) tetrafluoroborate spin-crossover system. *Chem. Phys. Lett.* **1984**, *105*, 1–4. [CrossRef]
16. Decurtins, S.; Gütlich, P.; Hasselbach, K.M.; Hauser, A.; Spiering, H. Light-induced excited-spin-state trapping in iron(II) spin-crossover systems—Optical spectroscopic and magnetic-susceptibility study. *Inorg. Chem.* **1985**, *24*, 2174–2178. [CrossRef]
17. Decurtins, S.; Gütlich, P.; Kohler, C.P.; Spiering, H. New examples of light-induced excited spin state trapping (LIESST) in iron(II) spin-crossover systems. *J. Chem. Soc. Chem. Commun.* **1985**, 430–432. [CrossRef]
18. Bonhommeau, S.; Molnar, G.; Galet, A.; Zwick, A.; Real, J.A.; McGarvey, J.J.; Bousseksou, A. One shot laser pulse induced reversible spin transition in the spin-crossover complex $[Fe(C_4H_4N_2)\{Pt(CN)_4\}]$ at room temperature. *Angew. Chem.* **2005**, *44*, 4069–4073. [CrossRef] [PubMed]
19. Matsuda, M.; Isozaki, H.; Tajima, H. Reproducible on-off switching of the light emission from the electroluminescent device containing a spin crossover complex. *Thin Solid Films* **2008**, *517*, 1465–1467. [CrossRef]
20. Titos-Padilla, S.; Herrera, J.M.; Chen, X.W.; Delgado, J.J.; Colacio, E. Bifunctional hybrid SiO_2 nanoparticles showing synergy between core spin crossover and shell luminescence properties. *Angew. Chem. Int. Ed.* **2011**, *50*, 3290–3293. [CrossRef] [PubMed]
21. Lacroix, P.G.; Malfant, I.; Real, J.A.; Rodriguez, V. From magnetic to nonlinear optical switches in spin-crossover complexes. *Eur. J. Inorg. Chem.* **2013**, *2013*, 615–627. [CrossRef]
22. Neville, S.M.; Halder, G.J.; Chapman, K.W.; Duriska, M.B.; Moubaraki, B.; Murray, K.S.; Kepert, C.J. Guest tunable structure and spin crossover properties in a nanoporous coordination framework material. *J. Am. Chem. Soc.* **2009**, *131*, 12106–12108. [CrossRef] [PubMed]
23. Coronado, E.; Gimenez-Marques, M.; Espallargas, G.M.; Rey, F.; Vitorica-Yrezabal, I.J. Spin-crossover modification through selective CO_2 sorption. *J. Am. Chem. Soc.* **2013**, *135*, 15986–15989. [CrossRef] [PubMed]
24. Munoz-Lara, F.J.; Gaspar, A.B.; Munoz, M.C.; Lysenko, A.B.; Domasevitch, K.V.; Real, J.A. Fast detection of water and organic molecules by a change of color in an iron(II) microporous spin-crossover coordination polymer. *Inorg. Chem.* **2012**, *51*, 13078–13080. [CrossRef] [PubMed]
25. Hassan, N.; Weinberger, P.; Mereiter, K.; Werner, F.; Molnar, G.; Bousseksou, A.; Valtiner, M.; Linert, W. Comparative investigations on a series of [hexakis(1-(tetrazol-1-yl)alkane-*N*4)iron(II)] bis(tetrafluoroborate) spin crossover complexes: Methyl- to butyl-substituted species. *Inorg. Chim. Acta* **2008**, *361*, 1291–1297. [CrossRef]
26. Gütlich, P. Spin crossover in iron(II)-complexes. *Struct. Bond.* **1981**, *44*, 83–195.
27. Franke, P.L.; Haasnoot, J.G.; Zuur, A.P. Tetrazoles as ligands Iron(II) complexes of monofunctional tetrazole ligands, showing high-spin reversible low-spin transitions. *Inorg. Chim. Acta* **1982**, *59*, 5–9. [CrossRef]
28. Dirtu, M.M.; Rotaru, A.; Gillard, D.; Linares, J.; Codjovi, E.; Tinant, B.; Garcia, Y. Prediction of the spin transition temperature in Fe^{II} one-dimensional coordination polymers: An anion based database. *Inorg. Chem.* **2009**, *48*, 7838–7852. [CrossRef] [PubMed]
29. Absmeier, A.; Bartel, M.; Carbonera, C.; Jameson, G.N.L.; Werner, F.; Reissner, M.; Caneschi, A.; Letard, J.F.; Linert, W. Mutual influence of spacer length and noncoordinating anions on thermal and light-induced spin-crossover properties of iron(II)-α,ω-Bis(tetrazol-1-yl)alkane coordination polymers. *Eur. J. Inorg. Chem.* **2007**, 3047–3054. [CrossRef]
30. Valtiner, M.; Paulsen, H.; Weinberger, P.; Linert, W. Theoretical investigations of a series of [hexakis(1-(tetrazol-1-yl)alkane-*N*4)iron(II)]bis(tetrafluoroborate) spin crossover complexes: Methyl-to-pentyl substituted species in the approximation of free cations. *Match-Commun. Math. Comput. Chem.* **2007**, *57*, 749–761.

31. Lucon, J.; Abedin, M.J.; Uchida, M.; Liepold, L.; Jolley, C.C.; Young, M.; Douglas, T. A click chemistry based coordination polymer inside small heat shock protein. *Chem. Commun.* **2010**, *46*, 264–266. [CrossRef] [PubMed]
32. Schweinfurth, D.; Demeshko, S.; Khusniyarov, M.M.; Dechert, S.; Gurram, V.; Buchmeiser, M.R.; Meyer, F.; Sarkar, B. Capped-tetrahedrally coordinated Fe(II) and Co(II) complexes using a "click"-derived tripodal ligand: Geometric and electronic structures. *Inorg. Chem.* **2012**, *51*, 7592–7597. [CrossRef] [PubMed]
33. Schweinfurth, D.; Demeshko, S.; Hohloch, S.; Steinmetz, M.; Brandenburg, J.G.; Dechert, S.; Meyer, F.; Grimme, S.; Sarkar, B. Spin crossover in Fe(II) and Co(II) complexes with the same click-derived tripodal ligand. *Inorg. Chem.* **2014**, *53*, 8203–8212. [CrossRef] [PubMed]
34. Fair, H.D.; Walker, R.F. *Energetic Materials*; Plenum Press: New York, NY, USA, 1977.
35. Lee, C.T.; Yang, W.T.; Parr, R.G. Development of the colle-salvetti correlation-energy formula into a functional of the electron-density. *Phys. Rev. B* **1988**, *37*, 785–789. [CrossRef]
36. Becke, A.D. Density-functional thermochemistry. III. The role of exact exchange. *J. Chem. Phys.* **1993**, *98*, 5648–5652. [CrossRef]
37. Stephens, P.J.; Devlin, F.J.; Chabalowski, C.F.; Frisch, M.J. Ab-initio calculation of vibrational absorption and circular-dichroism spectra using density-functional force-fields. *J. Phys. Chem.* **1994**, *98*, 11623–11627. [CrossRef]
38. Papai, M.; Vanko, G.; de Graaf, C.; Rozgonyi, T. Theoretical investigation of the electronic structure of Fe(II) complexes at spin-state transitions. *J. Chem. Theory Comput.* **2013**, *9*, 509–519. [CrossRef] [PubMed]
39. Cirera, J.; Paesani, F. Theoretical prediction of spin-crossover temperatures in ligand-driven light-induced spin change systems. *Inorg. Chem.* **2012**, *51*, 8194–8201. [CrossRef] [PubMed]
40. Droghetti, A.; Alfe, D.; Sanvito, S. Assessment of density functional theory for iron(II) molecules across the spin-crossover transition. *J. Chem. Phys.* **2012**, *137*. [CrossRef] [PubMed]
41. Reiher, M.; Salomon, O.; Hess, B.A. Reparameterization of hybrid functionals based on energy differences of states of different multiplicity. *Theor. Chem. Acc.* **2001**, *107*, 48–55. [CrossRef]
42. Ditchfield, R.; Miller, D.P.; Pople, J.A. Self-consistent molecular orbital methods. Molecular orbital theory of nmr chemical shifts. *J. Chem. Phys.* **1971**, *54*, 4186–4193. [CrossRef]
43. Armarego, W.L.F.; Chai, C.L.L. *Purification of Laboratory Chemicals*, 7th ed.; Butterworth-Heinemann Kidlington: Oxford, UK; Waltham, MA, USA, 2013.
44. Bruker Analytical X-ray Instruments, I. Available online: https://www.bruker.com/products (accessed on 19 February 2016).
45. Sheldrick, G.M. *Shelxs 97, Program. for the Solution of Crystal Structure*; University of Göttingen: Göttingen, Germany, 1997; Volume 125.
46. Sheldrick, G.M. *Shelxl 97, Program. for X-Ray Crystal Structure Refinement*; University of Göttingen: Göttingen, Germany, 1997.
47. Muttenthaler, M.; Bartel, M.; Weinberger, P.; Hilscher, G.; Linert, W. Synthesis and characterisation of new ditetrazole-ligands as more rigid building blocks of envisaged iron(II) spin-crossover coordination polymers. *J. Mol. Struct.* **2005**, *741*, 159–169. [CrossRef]